EFDA–JET–PR(09)02

T. Hirai, N. Bekris, J.P. Coad, C. Grisolia, J. Linke, H. Maier, G.F. Matthews,
V. Philipps, E. Wessel and JET EFDA contributors

Failure Modes of Vacuum Plasma Spray Tungsten Coating Created on Carbon Fibre Composites under Thermal Loads

Failure Modes of Vacuum Plasma Spray Tungsten Coating Created on Carbon Fibre Composites under Thermal Loads

T. Hirai[1]*, N. Bekris[2], J.P. Coad[3], C. Grisolia[4], J. Linke[1], H. Maier[5], G.F. Matthews[3], V. Philipps[1], E. Wessel[1] and JET EFDA contributors*

JET-EFDA, Culham Science Centre, OX14 3DB, Abingdon, UK

[1] Forschungszentrum Jülich EURATOM-Association FZJ, D-52425 J¸lich Germany
[2] EFDA CSU, Culham Science Centre, Abingdon Oxfordshire OX14 3DB UK
[3]EURATOM-UKAEA Fusion Association, Culham Science Centre, OX14 3DB, Abingdon, OXON, UK
[4] Association Euratom-CEA, Cadarache DSM/DRFC, F-13108 St-Paul-lez-Durance France
[5] Max-Planck-Institut für Plasmaphysik, EURATOM Association, Garching bei München Germany
** See annex of F. Romanelli et al, "Overview of JET Results",*
(Proc. 22[nd] IAEA Fusion Energy Conference, Geneva, Switzerland (2008)).

Preprint of Paper to be submitted for publication in
Journal of Nuclear Materials

ABSTRACT.
Vacuum Plasma Spray tungsten (VPS-W) coating created on a Carbon Fibre reinforced Composite (CFC) was tested under two thermal load schemes in the electron beam facility to examine the operation limits and failure modes. In cyclic ELM-like short transient thermal loads, the VPS-W coating was destroyed sub-layer by sub-layer at 0.33GW/m^2 and 1ms pulse duration. At longer single pulses, simulating steady state thermal loads, the coating was destroyed at surface temperatures above 2700^{o}C by melting of the rhenium containing multilayer at the interface between VPS-W and CFC. The operation limits and failure modes of the VPS-W coating in the thermal load schemes are discussed in detail.

1. INTRODUCTION

The primary ITER materials choice is a full beryllium (Be) main chamber wall with Carbon Fibre reinforced Composite (CFC) at the strike points and tungsten (W) at the dome and the upper part of the divertor vertical targets. Neither the reference material combination (Be Wall/ CFC+W divertor) nor its possible combination in the future (Be Wall/ W divertor) have ever been tested in a tokomak. Therefore, the ITER-Like Wall (ILW) Project has been launched at the JET tokamak [1,2]. The lessons we can learn from such an experiment in JET would be invaluable for reducing the risk of plasma-facing material related problems in ITER.

In ILW Project, the JET tokamak will employ tungsten coated CFC tiles for the outer and inner divertor rows. For this application, a 200μm thick Vacuum Plasma Spray (VPS)-W coating was selected at the end of R&D program in 2006 [3-6]. During normal JET operation the W coating at the JET divertor will be exposed to intense transient heat loads as well as to steady state thermal loads. Therefore, it is indispensable to assess the operation limit and failure modes of the coating under such thermal loading conditions.

In the present work, the operation limits and failure modes of the coating was studied under high thermal loads, (1) ELM-like short transient thermal loads; (2) longer pulse loads simulating steady state thermal loads in the electron beam facility.

2. TUNGSTEN COATING FOR THERMAL LOADING TESTS

The 200μm W coating was produced by Vacuum Plasma Spray (VPS) technology [7], by Plansee AG. Thick coating was regarded to be advantageous since the major fraction of the heat dissipates in the thick coating before arriving at the interface. The characteristic heat propagation distance is considered to be in a rage of 100μm during 1 ms on accounting a lower thermal conductivity of the VPS-W coating than a solid W (e.g. the heat propagation distance in a solid W is estimated to be several hundreds μm in 0.5ms [8]). Thus, the coating interface is not exposed to the thermal fatigue caused by the multiple short transient thermal loads. In fact, thinner (4μm and 10μm) PVD-W coatings were much sensitive to such thermal loads since the each heat pulse affected the interfaces [3, 4].

The cross section around the coating interface is shown in Fig.1. The W coating has a sophisticated

interlayer consisting of Rhenium (Re) and W multilayer interlayer. The use of Re/W multi-layer interlayer was aimed to be a diffusion barrier against carbon preventing the formation of tungsten carbide in the main W coating [9,10]. The soft Re layers would also provide a compliant interface between the CFC and the hard W layers in the coating system. The multilayer interlayer was created by Physical Vapour Deposition (PVD) process by alternating the deposition sources and processes, i.e. Re layers by arc deposition process and W layers by sputtering deposition process [11]. The multi-layer consisted of optimized six layers; 10μm-Re, 2μm-W, 3μm-Re, 2μm-W, 2.5μm-Re and 1μm-W, starting from the CFC surface to W coating side. The VPS-W coating was created in vacuum at high temperature (During VPS process, the plasma torch delivers a power density in the order of 5MW/m^2 onto the CFC substrate). The high process temperature can cause complicated residual stresses in the coating due to anisotropic thermal expansion mismatches between the W coating and CFC substrate. In addition, this residual stresses can cause tensile cracks in the W coating even just after production [6].

The W coating sample was produced on two Directional Carbon Fibre reinforced Composite, (2D-CFC, DMS780 Dunlop). The CFC has a fibre-bundle architecture based on a cross-ply laminates (x- and y-directions). PAN (polyacrylonitrile) fibre-bundles are utilized for the laminates. These fibre-bundles guarantee the high mechanical strength and thermal conductivity of the CFC in the two directions along the fibre-bundles. The carbon fibres have an anisotropic thermal properties that are originated from the nature of pyrolitic graphite [12] and the CFC constituents [13]. Indeed, along the fibre direction, the thermal expansion is low (around 0-1×10^{-6} K^{-1}) and the thermal conductivity high, while in the fibre radial direction the thermal expansion is higher (10-13×10^{-6} K^{-1}) and the thermal conductivity lower. The CFC contains felt layers sandwiched between the two cross-ply laminates as a compliant layer. Both fibre-bundle layers and felt layers have typically about 0.5mm thickness. The W coating was produced at a CFC surface containing perpendicular and parallel PAN fibre-bundles.

For the thermal tests, a large flat area of a CFC block which was roughly the half size of a JET divertor tile (G7 tile), 100×300mm^2, was coated. It is worth mentioning that during VPS coating, the plasma torch moved across the surface to be coated from the starting point to end point and returned at the staring point [9]. During such a back and forth process, the atmosphere and substrate temperature have to be well controlled, especially for large surfaces, otherwise, sub-layers can be created by each pass of the plasma torch due to non-uniform stress and deposition of material from the halo of the plasma torch.

3. HIGH HEAT FLUX TEST IN THE ELECTRON BEAM FACILITY JUDITH

High Heat Flux (HHF) tests were performed by the electron beam facility, JUDITH, at the Forschungszentrum Jülich, Germany [14,15]. The maximum beam power is 60kW. The beam was focused to a diameter of approximately 1 mm. Fairly homogenous heat distribution is realized by fast scanning of the electron beam (typically 40kHz in x-direction and 31kHz in y-direction). The

maximum beam scanning area is 100×100 mm^2 at the test position. Absorbed power density was calculated as the product of the acceleration voltage and the absorbed beam current. The acceleration voltage was held constant and the beam current was varied to provide defined heat loads. Although, the acceleration voltage is high (120kV), the penetration depth of the electron beam in solid tungsten was calculated to be up to 5μm. Considering the thickness of coating (200μm), the loading can be regarded as a surface heat flux.

ELM-like short thermal loading was applied by a 1 ms pulse with a rectangular waveform over a well-defined area of 16 mm^2 at room temperature. This load was repeated for 1000 cycles. The bulk temperature increase of the W coated CFC block was negligible due to the large thermal mass of the CFC block. In this HHF tests, the power density limit and failure mode were examined. Longer pulses were applied over an area of 64mm^2 in order to simulate the steady state heat load. It was necessary to limit pulse duration and the loading area to realize high power density loads and minimize the energy deposition into the sample. The pulse duration was selected to be 2s which is much longer than the material time constant (characteristic time for heat propagation through the coating and interlayer to the CFC substrate). The loaded area was designed to cover several units of the underlying CFC laminate structure. Single pulse loads at virgin coating surfaces were applied at around room temperature. The bulk temperature increased up to 50^oC after the pulses. In this HHF test, the operational temperature limit and failure mode were examined.

The bulk temperatures were monitored with an infra-red camera, AGEMA THV900 (detection wavelength: around 3.5μm) through a CaF_2 window. In addition, the time evolution of the averaged surface temperature in a 3-4 mm diameter spot was observed with a single colour pyrometer (detection wavelength: around 1.5-1.6μm; detection limit 633^oC at emissivity 0.2) though a quartz window. In both cases, the emissivity was assumed to be 0.2 over the measured temperature range.

4. FAILURE MODE AND POWER DENSITY LIMITS OF VPS-W COATING UNDER ELM-LIKE SHORT TRANSIENT THERMAL LOADS

Figure 2(a) shows the time evolution of surface temperature loaded at 0.33GW/m^2 for 1ms, over 500 cycles. As it is illustrated in this figure, the maximum surface temperature for the first shot was around 1200^oC. Moreover, as expected the maximum surface temperature increases with the number of shots and reaches 2200^oC after 200 shots. The maximum surface temperature increased drastically at the beginning of the cyclic loading and it saturated at a later stage (Fig.2(b)). At higher power densities the temperature increase saturated at an earlier stage. This indicates the early completion of the coating destruction due to higher thermal stresses induced by higher power loads. Another remarkable finding was significant change of the cooling rates. After the first cycle, the surface temperature decreased rapidly whereas after the 50th cycle, one can observe a noticeable slow down of the cooling rate. This indicated a poor thermal contact of the coating layers to the underlying substrate leading to a less efficient heat removal.

Figure 3(a) shows the microstructure of the surface loaded at 1GW/m^2 1ms for 100 cycles. The

coating showed surface damage that consisted of small droplets and peeling of sub-layers of VPS-W coating. Numbers of cracks were generated at the loaded surfaces during the cyclic loading [16]. The sub-layers started to melt at the crack edges where the thermal masses were small. The micrograph (Fig.3(a)) indicates the destruction processes: (i) cracking of an upper sub-layer, (ii) melting of crack edges of the sub-layer, (iii) removal/ extraction of the sub-layer due to melting/ re-solidification of the molten sub-layer, (iv) cracking of the lower sub-layer due to thermal exposure, (v) melting of crack edges of the sub-layer.

Figure 3(b) and 3(c) show the cross section of the coating loaded at 0.4GW/m^2 after 200 pulses. As shown in Fig.3(b), a tensile crack [6] running through the entire VPS-W coating thickness existed before the experiments. The tensile crack width in the image was around 20μm. As shown in Fig.3(c), the VPS-W coating consisted of seven sub-layers. The coating was removed sub-layer by sub-layer due to the poor mechanical and thermal contact of each sub-layer. After removal/ delamination of the sub-layers, melting of the sub-layer occurred because of the small thermal masses of the detached layers. Two sub-layers were removed after 200 cycles at 0.4GW/m^2 for 1 ms loading. The same destruction process was observed after 500 cycles at 0.33 GW/m^2 for 1 ms. The sub-layer structure was not observed in previous tests of small samples (~80mm × ~80 mm). Indeed, the previous tests on the small sample did not show any damage after 1000 cycles at 0.33 GW/m^2 for 1ms [3]. The high resistance was likely associated with a monolithic structure of the thick coating without having sub-layers. It is concluded that the formation of the sub-layers during production process was the critical point, which is assumed to be the result of scaling the process to large areas where deposition from the halo of the plasma torch and surface temperature are not as easy to control. In such VPS process, each sub-layer corresponds to a single pass of the plasma torch across the tile surface.

Cracks developed horizontally in the CFC part were formed beneath the VPS-W coating layer due to poor mechanical stability. The cracks extended in a range of mm around the tensile cracks. These horizontal cracks caused an increase of the surface temperature and low cooling rate due to poor thermal contact. The multilayer did not show microstructural modification by the short pulse loading (Fig.3(c)) since the coating was thermally thick (the pulse duration was shorter than characteristic time for heat propagation through the coating to interlayer).

5. FAILURE MODE AND TEMPERATURE LIMITS OF VPS-W COATING UNDER STEADY STATE THERMAL LOADS

Figure 4 shows the time evolution of the surface temperature at the VPS-W coating. The coating did not show any damage below 103MJ/m^2 for 2s [16]. The destruction occurred above 113 MJ/m^2 for 2s. The measured averaged surface temperature at this energy density reached up to 3200^{o}C. The surface temperature showed a stagnation point at around 2700^{o}C (the temperature could be locally higher within the averaged surface area). This stagnation indicates melting of the coating. The temperature at the stagnation point was far below the melting temperature of W (3400^{o}C). This

is due to melting of the interlayer after W-Re alloy and/or WC formation which would be created by mutual diffusion in the multilayer at high temperature. The melting points of the W-Re alloy and WC go down to 2825°C and 2715°C, respectively [17]. This is the thermally weakest point in the coating system.

Figure 5(a) shows a microstructure of the surface loaded at 113MJ/m^2 for 2s. At this energy density the coating showed melting. Two holes with a distance of about 2mm were found at the loaded surface. This separation is due to the structure of the underlying CFC substrate as shown in Fig.5(b). CFC surfaces were found through the holes, which were caused by the poor wetting of the molten W alloy at carbon surface. This microstructure implies that melting started at multilayer interlayer around the CFC surface as discussed above. In the re-solidified layer at the top surface, W as well as small amount of Re and C were detected by Energy Dispersive Spectrometry (EDS) analysis [16].

The coating did not show any remarkable damages, e.g. melting, cracking, below the energy density. It indicates that the coating had a clear damage threshold which defined by the surface temperature. One must note that the threshold energy density is not relevant in this experiment since the energy dissipates in a large thermal mass of the sample after deposited at a small loaded area. Thermal loading at the entire sample surface was required to define the threshold energy density [18], which was considered in these experiments.

Figure 5(b) and 5(c) show cross section of the damaged VPS-W coating. The section line was near the crater. As mentioned above, the melting of the coating depends on the underlying CFC structure. Figure 5(b) shows that the coating melted at the fibre-bundle parallel to the surface where the heat transfer into the bulk was low. Here was the starting point of melting due to overheating. Severe melting was observed at the interlayer as shown in Fig.5(c). Above the molten layer at around interlayer, VPS-W sub-layers could still be observed and appear unaffected. This microstructure confirms that the destruction of the coating started by melting at the interlayer but not at the top surface. At the top surface, a re-solidified layer was observed, which was originated from the surrounding crater near the section line. Consequently, the destruction processes of the coating under steady state thermal loads are: (i) overheating at the parallel fibre-bundles of CFC substrate; (ii) decrease of melting temperature by formation of W-Re alloy and/or WC in the multilayer interlayer; (iii) melting of the interlayer; (iv) mass transport of molten W-Re phase during heating; (v) cavities formation during cooling phase. The poor wetting of the molten W alloy at carbon surface caused the large crater and open carbon surfaces at the damaged area.

SUMMARY AND CONCLUDING REMARKS

Thermal load tests were performed on a 200μm Vacuum Plasma Spray (VPS) W coating created at 2D CFC with W/Re multilayer interlayer. The thermal load tests were multiple short pulse loading, i.e. ELM-like short transient thermal load tests, and longer single pulse loading, i.e. steady state thermal load tests.

Under ELM-like short transient thermal loads, the coating showed surface damages such as small droplets and peeling of sub-layers in VPS-W layers. The damage threshold in power density was below 0.33 GW/m^2 1ms. The formation of the sub-layers was the critical point with respect to the performance of the VPS-W coating under the ELM-like thermal loads. Under steady state thermal loads, the coating showed melting of the multilayer interface at the locally overheated parallel fibre-bundles. The formation of W-Re alloy and/or WC caused decreases of melting point. The damage threshold in operation temperature was found to be the melting points of W-Re alloy (2825^{o}C) and/or W-C (2715^{o}C).

As a result of numbers of experimental observations, ILW Project made a decision to dismiss the 200 μm VPS-W coating from the Project baseline. Thinner PVD-W coatings are being developed and qualified for the ILW Project [19].

ACKNOWLEDGEMENTS

Authors would like to thank Mr. V. Gutzeit for his supports in the metallographic study of the coating. This work, supported by the European Communities under the contract of Association between EURATOM/FZJ, was carried out within the framework of the European Fusion Development Agreement. The views and opinions expressed herein do not necessarily reflect those of the European Commission.

REFERENCES

[1]. J. Pamela, G.F. Matthews, V. Philipps, R. Kamendje, JET-EFDA Contributors, "An ITER-like wall for JET" J. Nucl. Mater. **363–365** (2007) 1–11.

[2]. G.F. Matthews, P. Edwards, T. Hirai, M. Kear, A. Lioure, P. Lomas, A. Loving, C. Lungu, H. Maier, P. Mertens, D. Neilson, R. Neu, J. Pamela, V. Philipps, G. Piazza, V. Riccardo, M. Rubel, C. Ruset, E. Villedieu and M. Way, Physica Scripta, T**128** (2007) 137-143.

[3]. T. Hirai, H. Maier,M. Rubel, Ph. Mertens, R. Neu, E. Gauthier, J. Likonen, C. Lungu, G. Maddaluno, G.F.Matthews, R.Mitteau, O. Neubauer, G. Piazza, V. Philipps, B. Riccardi, C. Ruset, I. Uytdenhouwen, JET EFDA Contributors, R&D on full tungsten divertor and beryllium wall for JET ITER-like wall project, Fusion Eng. Des. **82** (2007) 1839–1845.

[4]. H. Maier, T. Hirai, M. Rubel, R. Neu, Ph. Mertens, H. Greuner, Ch. Hopf, G.F. Matthews, O. Neubauer, G. Piazza, E. Gauthier, J. Likonen, R. Mitteau, G. Maddaluno, B. Riccardi, V. Philipps, C. Ruset, C.P. Lungu, I. Uytdenhouwen, JET EFDA contributors, Tungsten and beryllium armour development for the JET ITER-like wall project, Nucl. Fusion **47** (2007) 222–227.

[5]. R. Neu, H. Maier, E. Gauthier, H. Greuner, T. Hirai, Ch. Hopf, J. Likonen, G. Maddaluno, G.F. Matthews, R. Mitteau, V. Philipps, G. Piazza, C. Ruset, JET EFDA Contributors, Investigation of tungsten coating on graphite and CFC, Phys. Scr. T**128** (2007) 150–156.

[6]. H. Maier, R.Neu, H. Greuner, Ch. Hopf, G.F. Matthews,G. Piazza, T. Hirai, G. Counsell, X.

Courtois, R. Mitteau, E. Gauthier, J. Likonen, G. Maddaluno, V. Philipps, B. Riccardi, C. Ruset, EFDA-JET team, Tungsten coating for JET ITER-like wall project, J. Nucl. Mater. **363–365** (2007) 1246–1250.

[7]. R. B. Heimann, "Plasma spray coating : principles and applications", Weinheim: Wiley-VCH , 2008, ISBN 978-3-527-32050-9.

[8]. T. Hirai, G. Pintsuk, Fusion Engineering and Design **82** (2007) 389–393.

[9]. ITER Material assessment report 2001 G **74** MA 10 W0.3.

[10]. H. Maier, Materials Science Forum **475-479** (2005) 1377-1382.

[11]. H. Maier, J. Luthin, M. Balden, S. Lindig,J. Linke,V. Rohde, H. Bolt, ASDEX Upgrade Team, Journal of Nuclear Materials **307–311** (2002) 116–120.

[12]. B. T. Kelly, Physics of graphite, Applied science publishers, 1981.

[13]. G. Savage, Carbon-carbon composites, 1st ed., Chapman and Hall, 1993.

[14]. R. Duwe, W. K¸hnlein and H. M¸nstermann: Proc. 18th Symposium on Fusion Technology (SOFT), Karlsruhe Germany, (1994) **355-358**.

[15]. T. Hirai, K. Ezato, P. Majerus, "ITER Relevant High Heat Flux Testing on Plasma Facing Surfaces", Materials Transactions, Vol.**46** (2005) 412- 424.

[16]. T. Hirai, "Study of failure modes of JET tungsten coatings under multiple transient heat loads and steady state loads" JW6-FT-3.35 final report, IEF2-TN/12-2008.

[17]. T. B. Massalski, H. Okamoto, P. Subramanian, L. Kacprzak, "Binary alloy phase diagrams", ISBN0-87170-430-X, 1990, William W. Scott, Jr.

[18]. T. Hirai, J. Linke, M. Rubel, J.P. Coad, J. Likonen, C.P. Lungu, G.F. Matthews, V. Philipps, E. Wessel, JET-EFDA contributors, Fusion Engineering and Design **83** (2008) 1072–1076.

[19]. G.F. Matthews, J.P. Coad, H. Greuner, M. Hill, T. Hirai, J. Likonen, H. Maier, M. Mayer, R. Neu, V. Philipps, R. Pitts, V. Riccardo, and the ITER-like Wall Team "Development of Divertor Tungsten Coatings for the JET ITER-like Wall", Proc. 18th Int. Conf. on Plasma-Surface Interactions in Controlled Fusion Devices (Toledo, 2008).

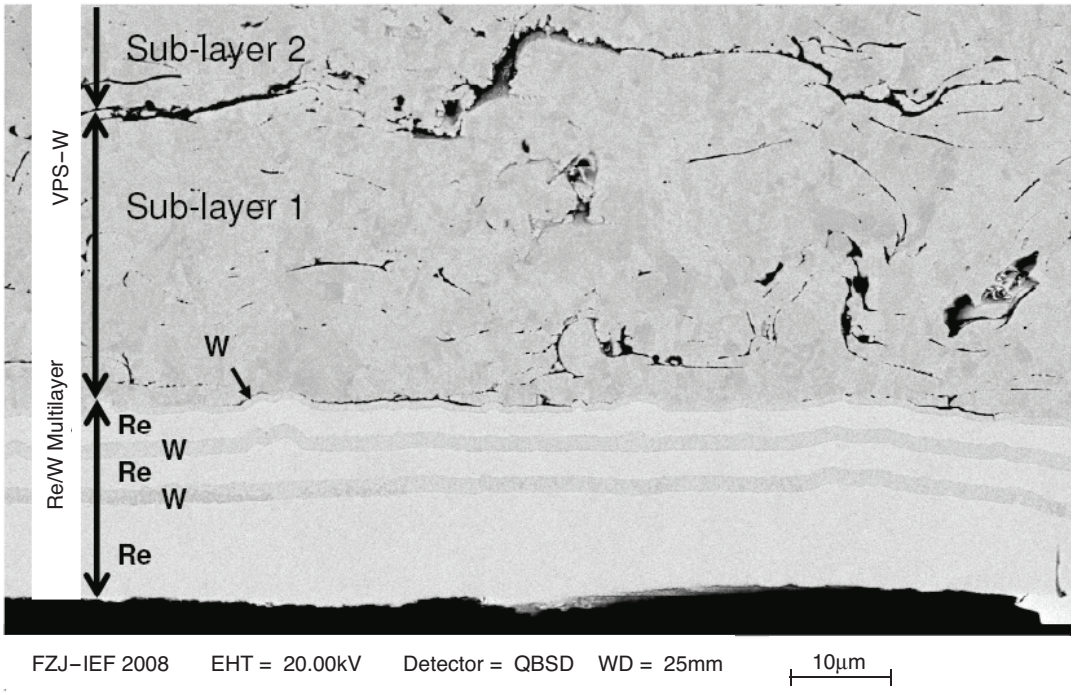

Figure 1: Cross section of the VPS-W coating and the multilayer interlayer.

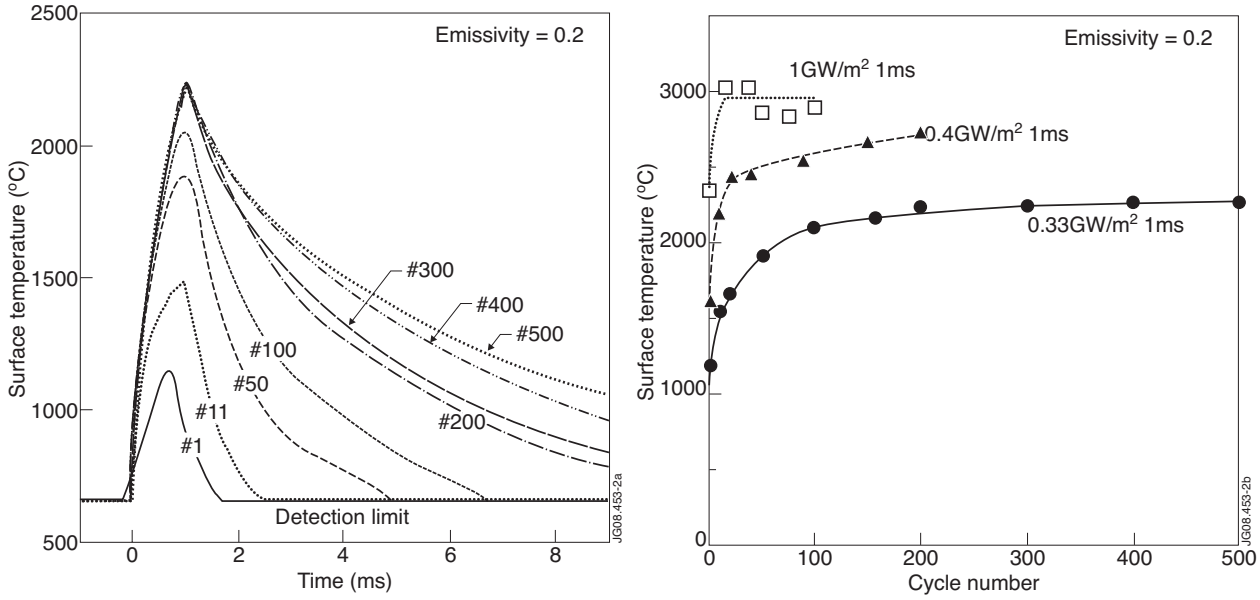

Figure 2: (left) Time evolution of surface temperatures under thermal loads at 0.33GW/m^2 1ms during cyclic loads. Note that the data acquisition was triggered by a defined surface temperature level. Due to the slow temperature increase, the date acquisition of the first pulse started later. Therefore, the pulse duration of the first shot appeared to be short, although the pulse duration was the same as the following shots. (right) Maximum surface temperature as a function of cycle number at the surfaces loaded at 0.33GW/m^2, 0.4GW/m^2, 1GW/m^2 for 1ms.

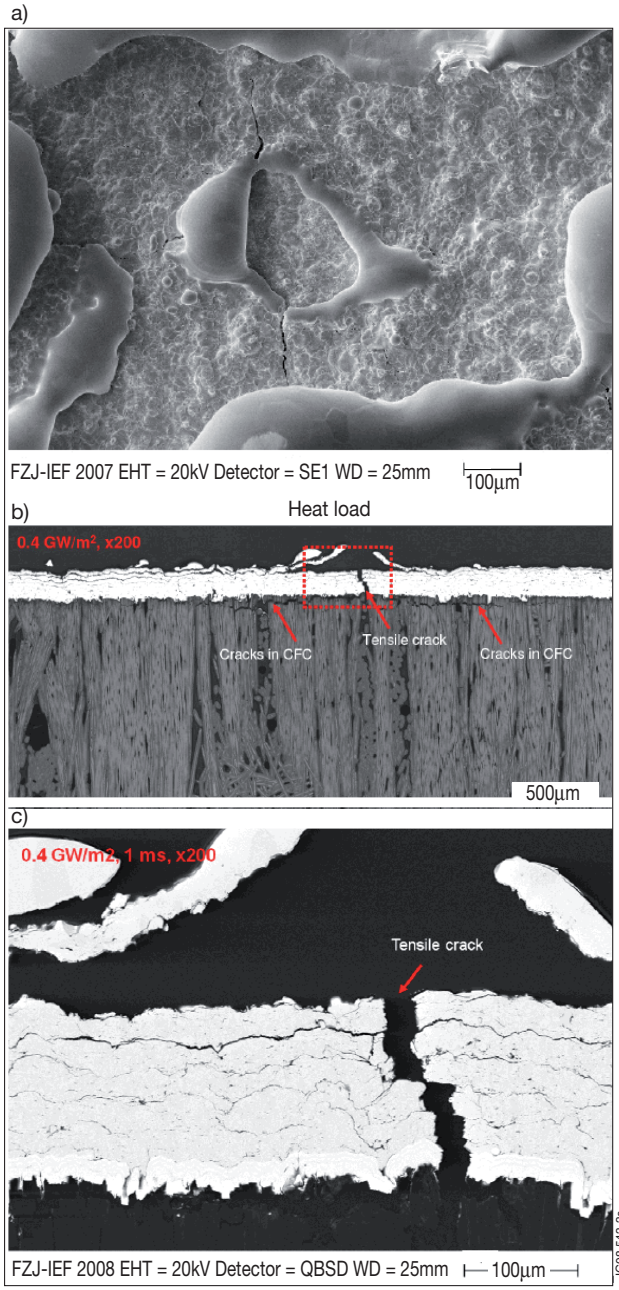

Figure 3: (a) Microstructure of the loaded surface at 1GW/m^2 for 1ms over 100 cycles, (b) and (c) cross section of the loaded area at 0.4GW/m^2 for 1ms over 200 cycles.

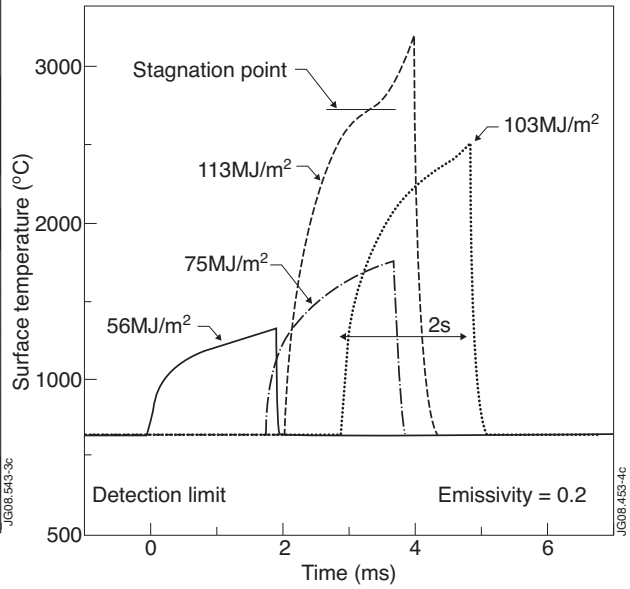

Figure 4: Time evolution of the surface temperature during steady state loads for 2s.

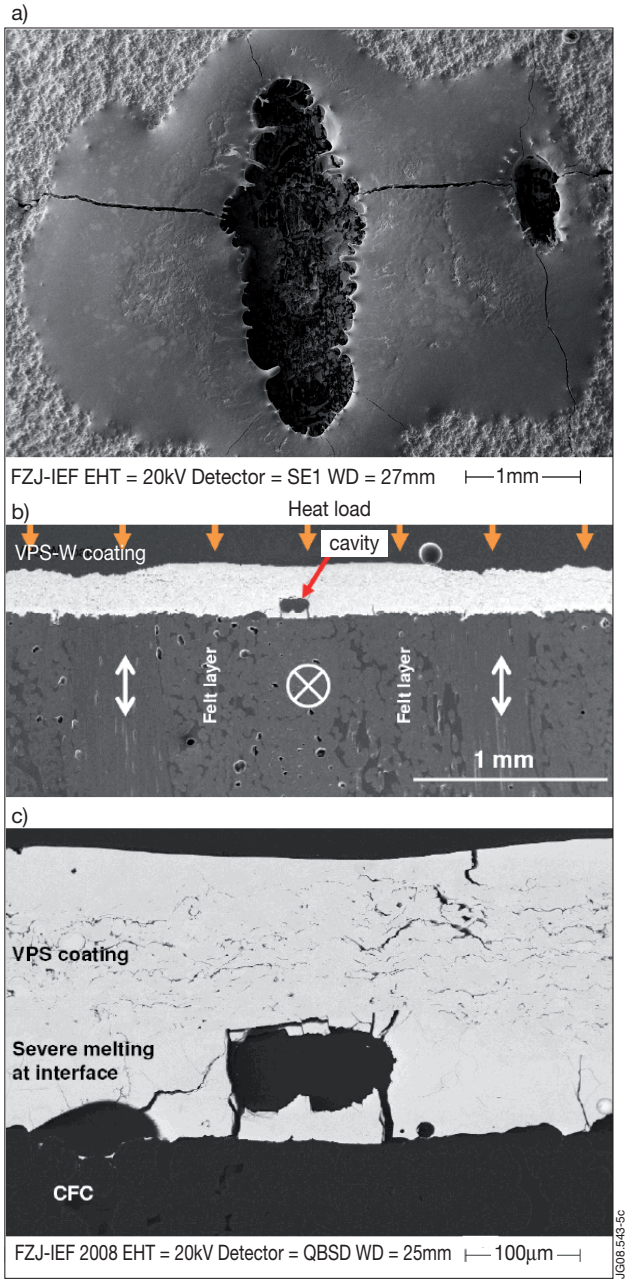

Figure 5: Microstructure of the loaded area at 113MJ/m^2 for 2s, single pulse, (a) microstructure of the loaded surface, (b) and (c) cross section of the loaded area at 113MJ/m^2 for 2s.